Laser and Particle Beams (2007), *25*, 85–91. Printed in the USA.

DOI: 10.1017/S0263034607070140

Production of multi-MeV per nucleon ions in the controlled amount of matter mode (CAM) by using causally isolated targets

C. STRANGIO,[1] A. CARUSO,[2] D. NEELY,[3] P.L. ANDREOLI,[1] R. ANZALONE,[1] R. CLARKE,[3] G. CRISTOFARI,[1] E. DEL PRETE,[1] G. DI GIORGIO,[1] C. MURPHY,[3] C. RICCI,[1] R. STEVENS,[3] AND M. TOLLEY[3]

[1]Associazione EURATOM-ENEA sulla Fusione ENEA-Frascati, Italy
[2]Università Kore, Enna, Italy
[3]Central Laser Facilities, CCLRC Rutherford Appleton Laboratory, UK

(RECEIVED 29 September 2006; ACCEPTED 17 October 2006)

Abstract

In several experiments, faster ions were produced from the backside of solid targets irradiated by powerful laser pulses. The ion acceleration was considered due to the negative electrostatic sheath formed on the backside of the target (TNSA), or to the expansion wave starting at the backside surface, or to the expansion wave and to its embedded electrostatic rarefaction shock. In this experiment, ions have been generated by transferring energy to a controlled amount of mass before the target become transparent by gas dynamic expansion (controlled amount of mass mode (CAM)). The targets used were thin transparent disks *causally isolated* from the holder to trim down, during the interaction process, unwanted effects due to the surrounding parts. Two kinds of target corresponding to a different set of parameters were designed (LARGE and SMALL). Both targets were conceived to survive, in the actual contrast conditions, to the low power pulse forerunning the giant laser pulse, bigger margin but lower performances being assigned to LARGE. For comparison standard square foils under the same focusing conditions, were also studied (LARGE-LIKE and SMALL-LIKE irradiation).

Keywords: CAM mode; Causally isolated target; Fast ions; Ion acceleration

1. INTRODUCTION

In prior experiments, the fastest ions was generated from the backside of foils irradiated on the frontside by powerful short laser pulses (Hatchett *et al*., 2000; Clark *et al*., 2000; Borghesi *et al*., 2002, 2005; Roth *et al*., 2002, 2005; Brambrink *et al*., 2006; Hegelich *et al*., 2002; Allen *et al*., 2003; Matsukado *et al*., 2003; Shurokhov & Pukhov, 2004; Badziak *et al*., 2005, 2006). Explanations for this process were the ion-acceleration or in the negative electrostatic sheath formed on the backside of the target normal sheath acceleration (TNSA) (Hatchett *et al*., 2000), or in the expansion wave starting at the surface of the backside (Wilks *et al*., 2001), or in the expansion wave and in its embedded electrostatic rarefaction shock (Strangio & Caruso, 2005).

Address correspondence and reprint requests to: C. Strangio, Associazione EURATOM-ENEA sulla Fusione ENEA-Frascati, Frascati, Italy. E-mail: strangio@frascati.enea.it

In our experiment, the fast ions were generated by irradiating a controlled amount of mass (CAM mode) (Caruso & Gratton, 1971; Caruso & Strangio, 2001). In the CAM mode for a given target thickness, the laser spot area need to match the target surface corresponding to the predetermined value of m. As a result of the target design, near field focusing was required in our experiment to get the proper irradiation conditions in the above-mentioned sense.

The targets used were thin transparent Si_3N_4 disks, produced as a whole from the same foil with 2 or 3 spokes of length L and width w anchored to a massive support (Fig. 1). An upper limit to the width w was set by requiring the total mass in the spokes to be smaller than that of the disk. The spoke length was $L > ct/2$, where c is the speed of light and t is any time of interest for the interaction process under scrutiny (e.g., pulse duration, expansion time, etc. . .). Under this condition, the time of a round trip of any information between the target and the massive support is longer than t, and unwanted effects due to the surrounding parts are trimmed

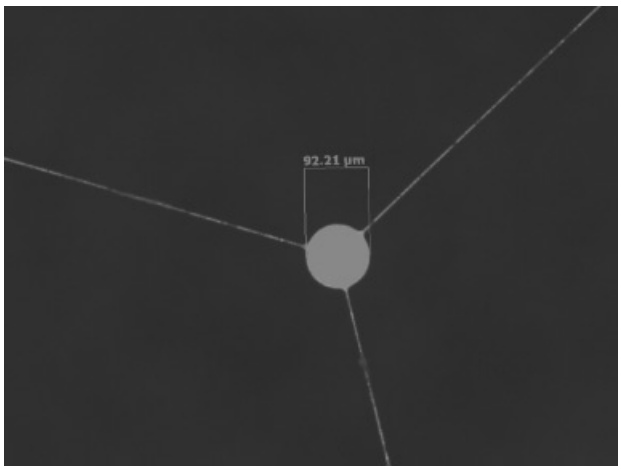

Fig. 1. An example of a causally isolated target fabricated by using microelectronics techniques and dimensioned according to the prescriptions in the text. The disc to be irradiated is suspended by strips $1 \div 2$ μm wide and same thickness and material as the disk.

down. This result in a *causally isolated target* being the additional mass possibly involved in the interaction smaller than the mass of the disk, and no return current can affect the fast electrons confinement in the time of interest. Under these conditions, if a large majority of the fast electrons generated in the experiment are trapped in the target, their energy will be ultimately transferred to the ions via the quasi-neutrality electrostatic field that couples electrons to ions, and drives the target expansion. The average specific energy (energy per nucleon) transmitted in this process to the ions will be $E_{nucl} = \eta_{tr}(E_{laser}/m)M_o$, where η_{tr} is the fraction of the laser pulse energy (E_{laser}) transferred to the target, and M_o is the mass of the nucleon. If E_{laser} and the desired E_{nucl} are assigned, then the allowed mass is $m = \eta_{tr} M_o(E_{laser}/E_{nucl})$.

The initial target parameters, radius R_o, thickness Δ_o, and density ρ_o (3.25 g/cm^3 for Si_3N_4), were assigned to render the target aspect ratio $q = \rho_o/\rho_c$, where $q \equiv 2R_o/\Delta_o$ and ρ_c are the critical density for the fully ionized material (Caruso & Strangio, 2001). In the experiment, the laser wavelength is $\lambda = 1.054$ μm, and results $q \approx 967$. Therefore, the targets are initially very thin flat disks and become transparent to the laser light when, due to gas-dynamic expansion, their thickness results $\Delta_c \approx 2R_o$, at a time $t = t_c$. An estimate of t_c is $t_c \approx R_o/(V_o/2)$ where $V_o = \sqrt{2E_{nucl}/M_o}$. Since the useful time for energy transfer to the target is $t \leq t_c$, then t_c represents an upper limit for the laser pulse duration t_{laser}. Simple calculations along this scheme show that the target dimensions (R_o, Δ_o), scale as $(E_{laser}/E_{nucl})^{1/3}$, the maximum allowed t_{laser} as $E_{laser}^{1/3}/E_{nucl}^{5/3}$, and the on-target power density (I) as $E_{nucl}^{3/2}$ (see Caruso & Strangio, 2001; Strangio & Caruso, 2005). The last dependence indicates that in the CAM mode, the power density I is mainly determined by the aimed E_{nucl}. Also, it is noted how the target dimensions and the laser pulse duration scale both as $E_{laser}^{1/3}$, so that for applications where high-energy pulses are required to generate a large number of ions, no very short laser pulses or extremely small targets or tight focusing are necessarily needed.

2. EXPERIMENT AND DATA ANALYSIS METHOD

For the available drive laser pulse energy, $E_{laser} \approx 170$ J delivered to the target in 1 ps, two kinds of CAM targets were designed assuming absorption efficiency $\eta_{tr} = 0.3$ and laser spot matching target diameter. Both targets (hereafter named LARGE and SMALL) were designed to survive, in the actual contrast conditions, to the pre-pulse forerunning the main laser pulse (Strangio *et al.*, 2004). In this context, for SMALL was chosen $2R_o \approx 32$ μm resulting in $\Delta_o \approx 40$ nm, $E_{nucl} \approx 5$ MeV/nucl, and $t_c \approx 1$ ps, while a bigger survival margin but lower performances were assigned to LARGE ($2R_o \approx 92$ μm, $\Delta_o \approx 100$ nm, $E_{nucl} \approx 0.25$ MeV/nucl, $t_c \approx 13$ ps).

For SMALL, the expansion time turns-out to be of the same order as the available laser pulse duration t_{laser}, and the energy flows to the ions while is supplied to the fast electrons. The radiation pressure transfers to the system a specific energy in the order of 0.5 MeV/nucl, while the light penetration into the target (estimated as c/ω_p, including relativistic effects) results in $0.25\ \Delta_o$. Therefore, the electromagnetic field interacts, from the beginning, with the electrons deep in a significant portion of the over-dense target volume. This circumstance can be relevant for the physics possibly involved (Yin *et al.*, 2006).

For comparison, standard 5×5 mm^2 square foils with a thickness of 50 and 100 nm, under the same focusing conditions, were irradiated by laser spots of 30 μm and 90 μm diameter (SMALL-LIKE and LARGE-LIKE irradiation). A shot on the isolated target SMALL was also performed in the tight focusing mode (SMALL-TIGHT: estimated laser spot diameter < 10 μm). All the targets were irradiated before focus, at an angle of 27° with respect to the target normal, by a $f/3$ aperture beam. A plasma mirror ($\approx 55\%$ efficiency, Ziener *et al.*, 2002) was used to obtain a contrast in excess of 10^9 between the nanosecond-forerunner and the main laser pulse (Fig. 2).

Due to the large target aspect ratio, most of the ions were expected in the directions close to the normal to the target, on both sides. Six Thomson spectrometers of peculiar design (Bandyopadhay *et al.*, 2006) detected ions at angular positions P_θ, where θ is measured counter-clockwise starting from the backward normal to the target (Fig. 3). Ions were registered on CR39 plates as pits along parabolas in a (x, z) plane (a parabola corresponds to a charge to mass ratio Z/A and a point on a parabola corresponds to a value of ion specific energy E_{nucl}).

A software package (Strangio, 2006) was prepared for ion data analysis of this experiment. For each spectrometer, after matching the experimental pit pattern to the expected

https://doi.org/10.1017/S0263034607070140 Published online by Cambridge University Press

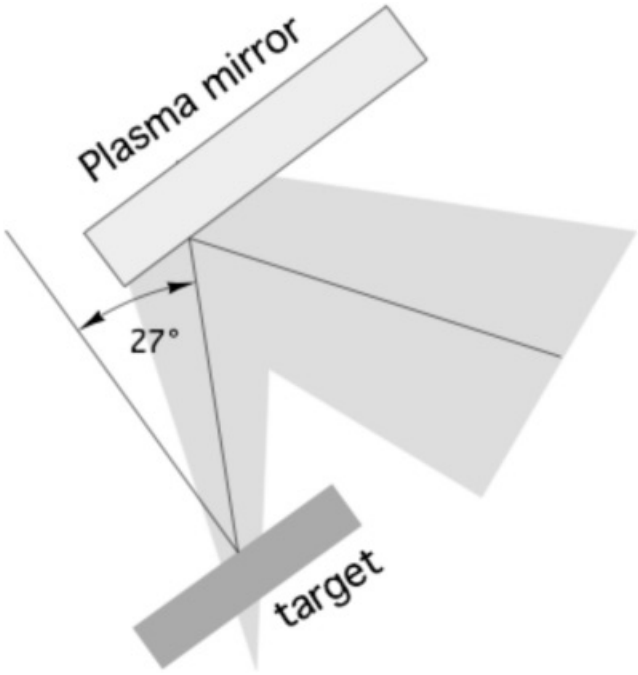

Fig. 2. The irradiation geometry. The laser beam is focused on the target by an $f/3$ parabolic optics via a plasma mirror introduced to improve the pulse contrast to a value $>10^9$. This is necessary to avoid target destruction by the nanosecond forerunner before the giant short pulse arrival. Contrast before plasma mirror was monitored shot by shot and was of the order of 10^8. The required spot sizes were obtained placing the target before beam waist.

theoretical curves, the ion species were individuated. In Figure 4 is given an example of pits displayed in the conjugate planes (x, z) and $(E_{nucl}, Z/A)$ after origin and fields direction individuation. This pattern was obtained by the spectrometer in position P_0 for a shot on a target LARGE. For each parabola, the average specific energy $\bar{E}_{nucl}$ and the spread $\Sigma_E = \sqrt{\langle (E_{nucl} - \bar{E}_{nucl})^2 \rangle}/\bar{E}_{nucl}$ were evaluated by the related experimental distribution function $f(E_{nucl})$. For each shot, the total number of ions collected by each spectrometer was interpolated by a function $g(\cos\theta)$, under condition $g(0) = 0$ (see Fig. 5 where g is measured in Tp/sr,

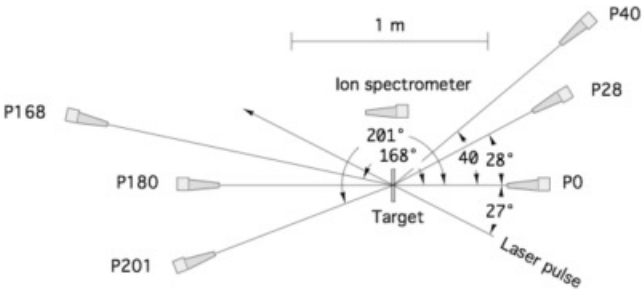

Fig. 3. Layout of the six Thomson ion spectrometers used in the experiment. The spectrometers were arranged in two clusters near the backward and the forward normal to the target.

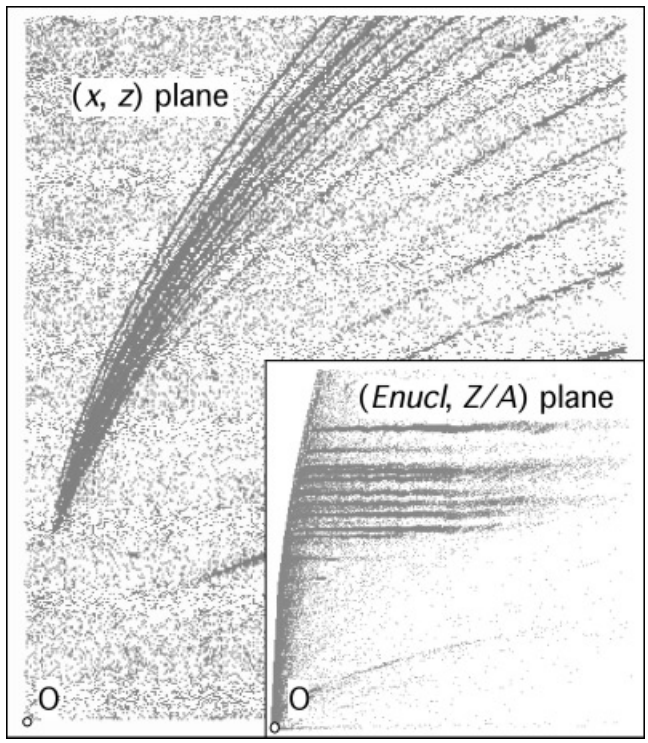

Fig. 4. Ion pits position on the CR39 plate (x, z) and on the plane energy per nucleon (E_{nucl}), specific charge (Z/A). The positions are represented after pattern recognition by matching experimental parabolas to the theoretical ones. The coordinate's origin is set coincident with the common parabolas vertex and the x-axis is taken on the common parabolas axis. Under such conditions only in the plane $(E_{nucl}, Z/A)$ the parabolas transform to straight lines parallel to the E_{nucl}-axis. The represented spectrum refers to a target "LARGE" and was registered at position P0 (backward normal to the target).

1 Tp = 10^{12} particles). The total number of detected ions was estimated by $2\pi \int_{-1}^{1} g(\cos(\theta)\, d\cos(\theta))$. The angular specific energy distribution, the specific energy E_{av} averaged on the total number of detected ions, and the average velocity $(\approx (2E_{av}/M_o)^{1/2})$ were likewise estimated as well as a spread Σ_{av} around E_{av}.

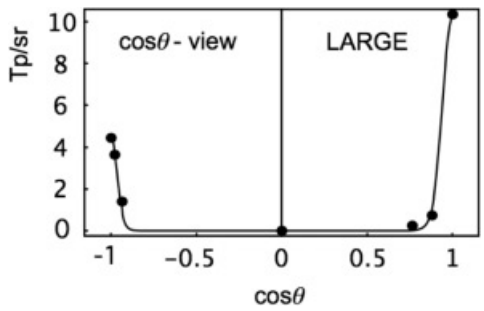

Fig. 5. Angular dependence of the number of ions emitted by a target. A fit was performed on the plane (Tp/sr, cos θ, where T/sr means Tera-particle/sterad) to perform the evaluation of the emitted particles number. Most of the ions are found around $\cos\theta = \pm 1$ since the prevalent emission is in direction near to the target normal.

https://doi.org/10.1017/S0263034607070140 Published online by Cambridge University Press

3. EXPERIMENTAL RESULTS

As expected from thin targets, most of the ionic emission occurred well collimated in the direction of the target normal. The relative amount of ions collected from the front-side and from the backside was target-type dependent, but typical and quite stable from shot to shot for a given target type.

The behavior of the total specific energy of the ions versus Z/A was analyzed. Ions were detected with $1/28 \leq Z/A \leq 1/2$. A typical value $Z/A \approx 1/3$ was found dividing the ions in a low energy group (LEG, $Z/A \leq 1/3$) and a high-energy group (HEG, $Z/A > 1/3$). LEG was typically found carrying a few percent of the total energy detected by the spectrometer, or empty. Ions from the target material were detectable as single component (all *odd*-Z Si except Si7) or in a binary mix (all N associated to *even*-Z Si) and only for $Z/A = 1/4$ and $Z/A = 1/2$ (two cases over fourteen) in a mixture with contaminants (C, O). Except for this two Z/A values, contaminants were detectable as single component (11 cases over 13). The *even*-Z Si population was inferred from the interpolation curve of the odd-Z Si ions versus Z. Then the N ions populations were obtained by subtracting the interpolated even-Z Si components from the related Si-N binary mixes (Fig. 6). Protons from contaminants with typical energy 2 MeV carrying out ≈15% of the total ion energy were also detected. Ions from contaminants and from target material were found with the same angular distribution as for LARGE and SMALL.

Table 1.

	LARGE	SMALL	LARGE-LIKE	SMALL-LIKE
E_{nucl}	0.01 ÷ 5	0.02 ÷ 35	0.01 ÷ 2.5	0.02 ÷ 5
$\bar{E}_{nucl}$	0.1 ÷ 1	0.05 ÷ 2.5	0.5 ÷ 1	0.02 ÷ 1
Σ_E	0.1 ÷ 0.5 (0.9)	≈ 0.5 (1)	0.2 ÷ 0.5	0.6 ÷ 0.9
E_{av}	0.5	1	0.5	0.5
Σ_{av}	0.5	0.5	0.5	0.5

Table 1 reports the range of the values for E_{nucl}, $\bar{E}_{nucl}$ with the related spread Σ_E, E_{av}, and Σ_{av} as found for LARGE, LARGE-LIKE, SMALL, and SMALL-LIKE irradiation. In many cases, for the isolated targets was found a spread $\Sigma_E \approx 0.9 \div 1$ corresponding to distribution functions strongly peaked around a low value of specific energy, and featured by a low-population high-energy tail (up to 5 MeV/nucl for LARGE and up to 35MeV/Nucl for SMALL, Fig. 7).

For LARGE, about 25% of the ions from the target material were detected from the target backside in direction close to the normal surface. The ion target content was 61.5 Tp, while the total number of detected ions, that included less than 10% of contaminants, was ≈ 6 Tp. Undetected ions are believed to be low energy ions not detectable by CR39, or stopped at the spectrometer by *E*-field plates, or deflected on the parabolas track portion extending outside of CR39 delimited area (Fig. 4). The resulting low-energy Z/A-dependent cutoff affects the measured E_{av} that comes-out

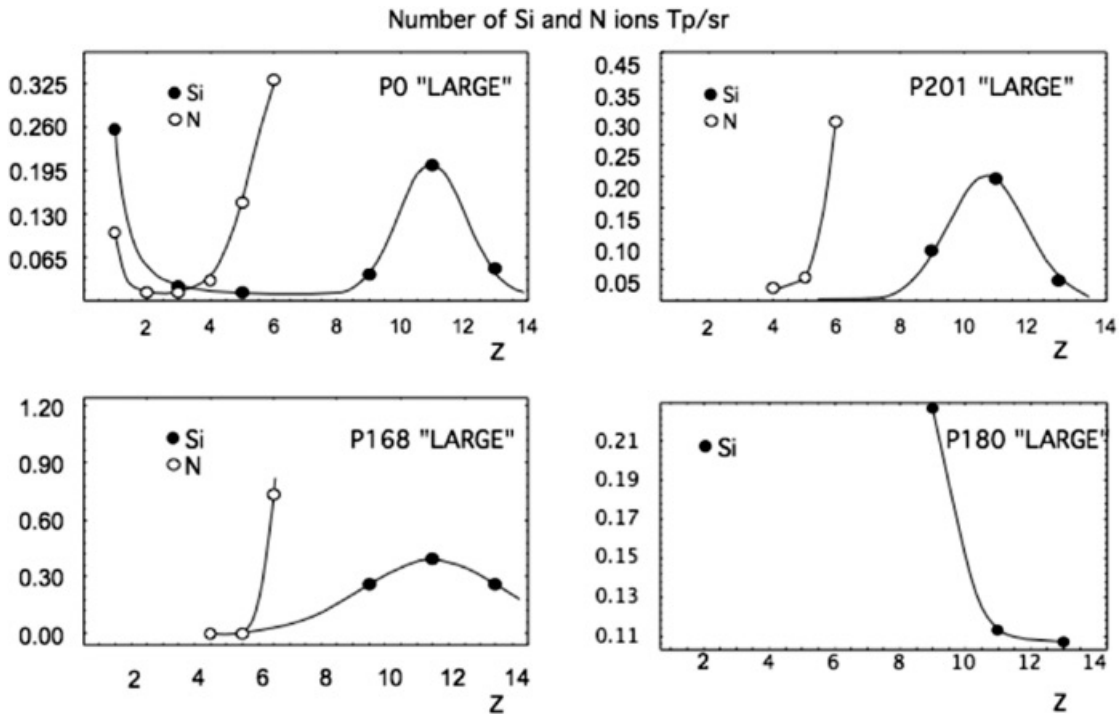

Fig. 6. Si and N ion populations (Tp/sr) as function of the charge number *Z*. The values for N were obtained by subtracting from Si-N mixes the number of the even ionized Si ions deduced from the Si population deduced by interpolation.

https://doi.org/10.1017/S0263034607070140 Published online by Cambridge University Press

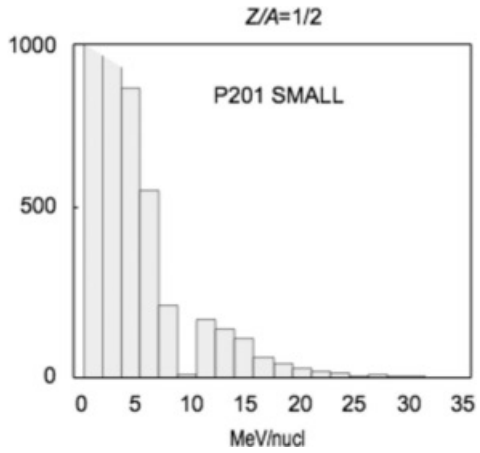

Fig. 7. A distribution function for target "SMALL" for the mix Z/A = 1/2. It noted the tail extending up to 35 MeV, an energy that for a Si ion corresponds to 35 × 28 = 980 MeV.

somewhat higher than expected. The average velocity measured for ions gives $t_c \approx 10 t_{laser}$. Therefore, on the average, the plasma density remains much higher than ρ_c while the electrons receive energy from the electromagnetic field.

The scenario for SMALL was different. Actually ions from the target material and contaminants corresponding to the higher ionization level (Z/A = 1/2) were found with energy up to 35 MeV/nucl in the P_{201} spectrometer, up to 10 MeV/nucl in P_{180} and P_{168}, up to 5 MeV/nucl in P_{28}. These ions reached energies between 0.4 and 1 GeV according to the value of their mass. Due to higher ion energy involved larger number of parabola tracks were completely caught in the CR39 area and the fraction of deflected ions outside the detection region resulted in lower than that for LARGE. The target ion nominal content was 3.15 Tp. The total number of detected ions was ≈ 1.5 Tp including contaminants C and O (carrying ≈50% of energy) and protons (carrying ≈15% of energy).

A value for E_{av} was found to be ≈1 MeV/nucl which is compatible with the huge presence of contaminants and with a fraction of absorbed energy η_{tr} on the order of 15%. A SMALL typical behavior is that most of the ions from the target material (≈ 70%), were emitted from the backside of the target and sampled at positions P_{168}, P_{180}, and P_{201}. This effect could be explained in terms of highly energetic ions emitted from the frontside of the target, but no ions with appropriate energy to balance the forward momentum were found on this side. Thus, the net forward momentum found in the experiment can be attributed to electrodynamics effects induced by the laser electromagnetic field (radiation pressure), that can overcome the thermokinetic effects in regimes of poor absorption, as in our case. Using the measured average ion velocity results $t_c \approx t_{laser}$. In this regime, the electrons give energy to the ions during the laser pulse absorption.

The shot on the isolated SMALL-TIGHT generated about 0.68 Tp, mainly ejected in the forward direction (80%) and energy between 0.2 and 2 MeV/nucl, while was found $E_{av} \approx$ 0.4 MeV/nucl. A few particles up to 20 MeV/nucl were found. Compared to SMALL, this energetically depressed scenario (in spite of tight focusing) probably came-out due to a hole drilled in the center of the disk by the forerunning nanosecond pulse. Under such conditions, the interaction of the main pulse was, for the central part of the spot, with rarefied, partially transparent plasma while the low-power density wings were interacting with an over-dense material.

The results for LARGE-LIKE were not significantly different from those obtained for LARGE except for the angular emission featured by ≈ 50% of ions detected from the rear-side of the target.

The scenario for SMALL-LIKE resulted in a different from that of typical SMALL. The value of E_{av} was lowered by a factor ≈2 and the time t_c increased up to $3t_{laser}$. Actually the measured ion energy range and the ion angular emission show a scenario similar to LARGE, where a fraction of low energy ions remained undetected. The total number of detected ions was ≈ 4.3 Tp from the target material (about 30% from the target backside) plus ≈ 0.7 Tp from contaminants. The fraction of detected ions (excluding contaminants) resulted 10% higher than the nominal target content (4 Tp) evaluated for a disk having the same radius as the nominal laser spot. For the isolated targets, the detected fraction of the initial particle content resulted in 0.5 for SMALL and 0.1 for LARGE. Thus, the real amount of ions involved in the interaction can be expected substantially higher than the measured one and corresponding to the matter within a radius greater than that of the nominal laser spot. These findings imply substantial transverse energy diffusion processes.

A crude estimate of the laser energy conversion efficiency to the fast ions η_{ions} was attempted by a modeling based on the only available ion experimental data. Actually a lower limit for η_{ions} was estimated due to the non-registered ions having energy $E_{nucl} < E_{cutoff}$. The amount of detected energy E_{ions} was estimated as $E_{ions} = N_{tot}\bar{A}E_{av}$, where N_{tot} is the total number of detected particle integrated over 4π and $\bar{A}$ is a suitable average over the species distribution of the detected particles. The total efficiency of the energy transfer to the ions resulted as $\eta_{ions} > 6\%$ for LARGE and $\eta_{ions} > 3\%$ for SMALL.

4. CONCLUSIONS

The production by short laser pulses of fast ions from solid targets of a new design was studied. An average energy of 170 J in 1 ps at $\lambda = 1.054\ \mu$m was delivered on a target after reflection by a plasma mirror to improve contrast ($>10^9$). Adopted targets were two kinds of ultra-thin, *causally isolated disks*. *Causally isolated disks* were supported by two spokes of negligible mass and of such a length to make the round trip of any information propagating at the speed of light between the target, and the massive support to last longer than all the physical process under scrutiny. Two kind

https://doi.org/10.1017/S0263034607070140 Published online by Cambridge University Press

of isolated target were adopted, SMALL (diameter 32 μm, thickness 40 nm) operated at 2×10^{19} W/cm^{-2} and LARGE (diameter 92 μm, thickness 100 nm) operated at 2.6×10^{18} W/cm^{-2}. Both targets were designed to survive to the pre-pulse, LARGE being more robust in this respect. Foils of similar thickness irradiated over the same spot size were also used for comparison (SMALL-LIKE, LARGE-LIKE).

In spite of the relatively modest power densities adopted, experiments demonstrated the production of ions with multi-MeV energy per nucleon, up to 5 MeV/nucl for LARGE and up to 35 MeV/nucl for SMALL. To be noted that for the mix where 35 MeV per nucleon were detected ($Z/A = 1/2$), this specific energy corresponds to an ion energy ranging from 0.4 to 1 GeV depending on the ion in the mix being considered. In all the experiments, most of the ion energy was found in ions with $Z/A \geq 1/3$. The group of ions with $Z/A < 1/3$ was or empty or carrying a modest amount of energy.

The physical scenario for SMALL and LARGE was different. By design, during the light absorption SMALL expanded over a distance on the order of its initial diameter, its density remaining greater than the critical one. For LARGE, the longitudinal expansion during irradiation resulted to be modest ($\approx$ 0.1 of its initial diameter). While for LARGE, more or less the same amount of ions (and energy) was collected on both sides of the target near its normal, for SMALL, a remarkable asymmetry was found, since most of the ions (and energy) were collected near the normal to the target in the forward direction, i.e., on the side opposite to the irradiated one. A source of momentum was required to explain this result and the most obvious was the light radiation pressure that can overcome the thermokinetic effects in the case of strong energy reflection ($\approx$ 85% energy reflection for our case).

The results for LARGE-LIKE were quite similar to those of LARGE, this indicating that causal isolation for that regime was non-influent. The situation is different for SMALL-LIKE, since with respect to SMALL, the specific energy was found degraded and the number of detected ions was larger than that subtended by the laser spot, this indicating a substantial transverse diffusion process. In addition, the strong asymmetry between the ions and the energy collected on both the target sides disappears. It is also interesting, the result obtained for an *isolated* target of the kind SMALL, irradiated in the tight focusing mode (SMALL-TIGHT, spot was ≈ 10 μm). In spite of tight focusing, SMALL-TIGHT was featured by a degraded specific energy scenario ($E_{av} \approx$ 0.4 MeV/nucl) probably due to the destruction of the target central portion by the pre-pulse, in spite of the high contrast obtained with the plasma mirror. The angular distribution of the ions and of their specific energy was quite similar to that of the isolated target SMALL, namely featured by a strong forward emission.

In conclusion we have performed a preliminary study on target to be operated in the controlled amount of mass mode. We believe that this irradiation mode could enable applications in a diverse range of fields from Inertial Confinement Fusion to nuclear physics.

ACKNOWLEDGMENTS

The experiment was supported by ENEA, the Italian National Agency for New Technologies, Energy and Environment and performed at Rutherford-Appleton Laboratory (RAL).

REFERENCES

Allen, M., Sentoku, Y., Audebert, P., Blazevic, A., Cowan, T., Fuchs, J., Gauthier, J.C., Geissel, M., Hegelich, M., Karsch, S., Morse, E., Patel, P.K. & Roth, M. (2003). Proton spectra from ultraintense laser–plasma interaction with thin foils: Experiments, theory, and simulation. *Phys. Plasmas* **10**, 3283–3289.

Badziak, J., Glowacz, S., Hora, H., Jablonski, S. & Wolowski, J. (2006). Studies on laser-driven generation of fast high-density plasma blocks for fast ignition. *Laser Part. Beams* **24**, 249–254.

Badziak, J., Glowacz, S., Jablonski, S., Parys, P., Wolowsky, J. & Hora, H. (2005). Laser-driven generation of high-current ion beams using skin-layer ponderomotive acceleration. *Laser Part. Beams* **23**, 401–409.

Bandyopadhay, S., Neely, D.G., Gianluca, A., Higgintbotham, D.C., MacKenna, P., Lindau, O., Lundh, F.O. & Wahlstrom, C.G. (2006). An analysis on the wedge-shaped Thomson spectrometer developed at Central Laser Facility. Oxfordshire, UK: Rutherford Appleton Laboratory.

Borghesi, M., Audebert, P., Bulanov, S.V., Cowan, T., Fuchs, J., Gauthier, J.C., MacKinnon, A.J., Patel, P.K., Pretzler, G., Romagnani, L., Schiavi, A., Toncian, T. & Willi, O. (2005). High-intensity laser-plasma interaction studies employing laser-driven proton probes. *Laser Part. Beams* **23**, 291–295.

Borghesi, M., Campbell, D.H., Schiavi, A., Willi, O., MacKinnon, A.J., Hicks, D., Patel, P., Gizzi, L.A., Galimberti, M. & Clarke, R.J. (2002). Laser-produced protons and their application as a particle probe. *Laser Part. Beams* **20**, 269–275.

Brambrink, E., Roth, M., Blazevic, A. & Schlegel, T. (2006). Modeling of the electrostatic sheath shape on the rear target surface in short-pulse laser-driven proton acceleration. *Laser Part. Beams* **24**, 163–168.

Caruso, A. & Gratton, R. (1971). On the possibility of producing 0.1 GeV ions by focusing ultrashort laser pulses on thin foils. *Phys. Lett.* **36A**, 275–276.

Caruso, A. & Strangio, C. (2001). Studies on nonconventional high-gain target design for ICF. *Laser Part. Beams* **19**, 295–308.

Clark, E.L., Krushelnick, K., Zepf, M., Beg, F.N., Tatarakis, M., Machacek, A., Santala, M.I.K., Watts, I., Norreys, P.A. & Dangor, A.E. (2000). Energetic heavy-ion and proton generation from ultraintense laser-plasma interactions with solids. *Phys. Rev. Lett.* **85**, 1654–1657.

Hatchett, S.P., Brown, C.G., Cowan, T.E., Henry, E.A., Johnson, J.S., Key, M.H., Koch, J.A., Langdon, A.B., Lasinski, B.F., Lee, R.W., MacKinnon, A.J., Pennington, D.M., Perry, M.D., Phillips, T.W., Roth, M., Sangster, T.C., Singh M.S., Snavely, R.A., Stoyer, M.A., Wilks, S.C. & Yasuike, K. (2000). Electron, photon, and ion beams

from the relativistic interaction of Petawatt laser pulses with solid targets. *Phys. Plasmas* **7**, 2076–2081.

Hegelich, M., Karsch, S., Pretzler, G., Habs, D., Witte, K., Guenther, W., Allen, M., Blazevic, A., Fuchs, Gauthier, J.C., Geissel, M., Audebert, P., Cowan, T. & Roth, M. (2002). MeV ion jets from short-pulse-laser interaction with thin foils. *Phys. Rev. Lett.* **89**, 085002-1/4.

Matsukado, K., Esirkepov, T., Kinoshita, K., Daido, H., Utsumi, T., Li, Z., Fukumi, A., Hayashi, Y., Orimo, S., Nishiuchi, M., Bulanov, S.V., Tajima, T., Noda, A., Iwashita, Y., Shirai, T., Takeuchi, T., Nakamura, S., Yamazaki, A., Ikegami, M., Mihara, T., Morita, A., Uesaka, M., Yoshii, K., Watanabe, T., Hosokai, T., Zhidkov, A., Ogata, A., Wada, Y. & Kubota, T. (2003). Energetic Protons from a Few-Micron Metallic Foil Evaporated by an Intense Laser Pulse. *Phys. Rev. Lett.* **91**, 215001-1/4.

Roth, M., Blazevic, A., Geissel, M., Schlegel, T., Cowan, T.E., Allen, M., Gauthier, J.C., Audebert, P., Fuchs, J., Meyer-ter-Vehn, J., Hegelich, M., Karsch, S. & Pukhov, A. (2002). Energetic ions generated by laser pulses: A detailed study on target properties. *Phys. Rev.* **5**, 061301-1/8.

Roth, M., Brambrink, E., Audebert, P., Blazevic, A., Clarke, R., Cobble, J., Cowan, T.E., Fernandez, J., Fuchs, J., Geissel, M., Habs, D., Hegelich, M., Karsch, S., Ledingham, K., Neely, D., Ruhl, H., Schlegel, T. & Schreiber, J. (2005). Laser accelerated ions and electron transport in ultra-intense laser matter interaction. *Laser Part. Beams* **23**, 95–100.

Shurokhov, O. & Pukhov, A. (2004). Ion acceleration in over-dense plasma by short laser pulse. *Laser Part. Beams* **22**, 19–24.

Strangio, C. & Caruso, A. (2005). Comparison of fast ions production modes by short laser pulses. *Laser Part. Beams* **23**, 33–41.

Strangio, C., Andreoli, P.L., Cristofari, G., Dattola, A. & Di Giorgio, G. (2004). A study for target modification induced by the prepulse in petawatt-class light-matter interaction experiments. *28th ECLIM Proceedings*.

Strangio, C. (2006). Inertial Confinement, *ENEA Nuclear Fusion Progress Report*.

Wilks, S.C., Langdon, A.B., Cowan, T.E., Roth, M., Singh, M., Hatchett, S., Key, M.H., Pennington, D., MacKinnon, A. & Snavely, R.A. (2001). Energetic proton generation in ultra-intense laser–solid interactions. *Phys. Plasmas* **8**, 542–549.

Yin, L., Albright, B.J., Hegelich, B.M. & Fernandez, J.C. (2006). GeV laser acceleration from ultrathin target. The laser break-out afterburner. *Laser Part. Beams* **24**, 291–298.

Ziener, C., Foster, P.S., Divall, E.J., Hooker, C.J., Hutchinson, M.H.R., Langley, A.J., Neely, D. (2002). The dependence of the specular reflectivity of plasma mirrors on laser intensity, pulse duration and angle of incidence. *Central Laser Facility Annual Report 2001/2002*.

https://doi.org/10.1017/S0263034607070140 Published online by Cambridge University Press